Spectroscopic constants and potential energy curves of 47 electronic states of InSb, InSb+, and InSb−

K. Balasubramanian

Citation: The Journal of Chemical Physics **93**, 507 (1990); doi: 10.1063/1.459551
View online: http://dx.doi.org/10.1063/1.459551
View Table of Contents: http://scitation.aip.org/content/aip/journal/jcp/93/1?ver=pdfcov
Published by the AIP Publishing

Spectroscopic constants and potential energy curves of 47 electronic states of InSb, $InSb^+$, and $InSb^-$

K. Balasubramanian[a)]
Department of Chemistry, Arizona State University, Tempe, Arizona 85287-1604

(Received 15 December 1989; accepted 19 March 1990)

Spectroscopic constants and potential energy curves of 26 electronic states of InSb, 12 electronic states of $InSb^+$, and 9 electronic states of $InSb^-$ are obtained using complete active space self-consistent field, first-order configuration interaction, second-order configuration interaction, and relativistic configuration interaction methods (CASSCF/FOCI/SOCI/RCI), including spin–orbit interaction. The SOCI calculations included up to 700 000 configurations. Spectroscopic constants obtained predict several allowed electronic transitions for InSb, $InSb^+$, and $InSb^-$ which are yet to be observed. The ground states of InSb, $InSb^+$, and $InSb^-$ are found to be $X\,^3\Sigma_{0^+}^-$, $X\,^4\Sigma_{1/2}^-$, and $X\,^2\Sigma_{1/2}^+$ with the constants InSb $X\,^3\Sigma_{0^+}^-$: $R_e = 3.02$ Å, $\omega_e = 121\ cm^{-1}$, $D_e = 1.35$ eV; $X\,^3\Sigma_1^-$: $R_e = 3.03$ Å, $\omega_e = 136\ cm^{-1}$, $T_e = 494\ cm^{-1}$; $InSb^+$ $X\,^4\Sigma_{1/2}^-$: $R_e = 3.351$ Å, $\omega_e = 63\ cm^{-1}$, $D_e = 0.37$ eV; and $InSb^-$ $X\,^2\Pi_{3/2}$: $R_e = 2.695$ Å, $\omega_e = 191\ cm^{-1}$, $D_e = 2.5$ eV. The adiabatic ionization potential and electron affinity of InSb are calculated as 6.33 and 1.41 eV, respectively. Analogous to the recently observed $A\,^3\Pi$–$X\,^3\Sigma^-$ system of GaAs, spectral bands in the 20 200 cm^{-1} region are predicted for InSb. Another $^3\Pi(II)$–$X\,^3\Sigma^-$ system is predicted at 15 830 cm^{-1}. Both the $^3\Pi$ states in these systems are found to be predissociated through crossing of a repulsive $^5\Sigma^-$ curve. The two low-lying electronic states of $InSb^-$ ($^2\Sigma_{1/2}^+$, $^2\Pi_{1/2}$) undergo relativistic avoided crossing.

I. INTRODUCTION

Generation and spectroscopic studies of Group III–Group V semiconductor clusters and their ions have received considerable attention in recent years.[1-29] The electronic properties of related Si_x, Ge_x clusters and their ions have also been the topic of several studies.[30-37] The study of mixed Group III–Group V clusters such as In_xSb_y, Ga_xAs_y, and In_xP_y are especially of great importance since Group III–Group V compounds are used in fast semiconductor devices. Mixed III–V clusters are especially intriguing due to their substantial difference in the fragmentation patterns and ionization behavior from the corresponding Group IV clusters, In addition the possibility of isomers even for small III–IV clusters[25] makes these species very interesting. Mixed clusters offer additional challenge to theoretical calculations as competing electronic states of the III and V atoms form an interesting array of electronic states.

The present author[10] carried out theoretical calculations on the electronic states of GaAs and $GaAs^+$. Theoretical prediction of a $^4\Sigma^-$ ground state for $GaAs^+$ was subsequently verified by an ESR spectrum of matrix-trapped $GaAs^+$ by Knight and Petty.[9] Theoretical prediction of an $X\,^3\Sigma^-$ ground state for the diatomic GaAs was recently verified by Lemire *et al.*[15] Meier *et al.*[16] made a SCF/MRDCI study on electronic states of GaAs and $GaAs^+$. More recently, an ambitious CASSCF/SOCI/RCI study which included up to 700 000 configurations on GaAs, $GaAs^+$, and $GaAs^-$ was made.[21]

Lemire *et al.*[19] have carried out a spectroscopic study of the diatomic GaAs using the supersonic jet expansion method. They found electronic bands attributed to the $^3\Pi(III)$–$X\,^3\Sigma^-$ system. The bands in this system were found to be predissociated due to crossing of a repulsive $^5\Sigma^-$ curve and the two excited $^3\Pi$ curves. With the exception of the $^3\Pi_{0^+}$–$X\,^3\Sigma^-$ system all other systems are predissociated. The results of theoretical calculations in Ref. 21 are in full accord with the experimental spectroscopic constants for GaAs obtained for $X\,^3\Sigma^-$ and $^3\Pi$ states.

O'Brien *et al.*[1] have studied Ga_xAs_y clusters generated by laser vaporization of GaAs crystal. Mass analysis of these clusters revealed considerable deviation from a binomial distribution for smaller clusters while large clusters followed the expected binomial distribution. Photofragmentation studies of $Ga_xAs_y^-$, Si_n^-, and Ge_n^- have also been made.[2,27] Ionization potentials of Ga_xAs_y clusters exhibited even–odd alternations. Kolenbrander and Mandich have recently studied In_xP_y clusters.[22]

There are no detailed spectroscopic studies on the diatomic InSb, $InSb^+$, and $InSb^-$ at present. In view of the considerable interest on Group III–V diatomics and clusters, the authors anticipates that such experimental studies are likely to be made in the near future. Duncan and coworkers are studying such mixed main group clusters. Knight and co-workers have communicated that they are investigating ESR spectra of a matrix isolated $InSb^+$ ion analogous to their earlier study on $GaAs^+$.[9] Due to significant experimental interest and since there are no experimental or theoretical studies on the diatomic InSb, $InSb^+$, and $InSb^-$ species, it was decided to carry out high-level *ab initio* calculations on potential energy curves of several electronic states of these species. We include both relativistic and elec-

[a)] Camille and Henry Dreyfus Teacher–Scholar.

 0021-9606/90/130507-13$03.00

tron correlation effects to a high order through CASSCF/FOCI/SOCI/RCI methods which included up to 700 000 configurations on InSb, $InSb^+$, and $InSb^-$. We compute potential energy curves of 26 electronic states of InSb, 12 electronic states of $InSb^+$, and 9 electronic states of $InSb^-$. Section II describes our method of theoretical calculations. Section III consists of results and discussions. Section IV comprises analyses of the nature of various electronic states, discussions on dipole moments, and Mulliken populations. Section V compares the computed properties of InSb with GaAs.

II. METHOD OF THEORETICAL CALCULATIONS

A complete active space MCSCF (CASSCF) method followed by first-order configuration interaction (FOCI) and second-order configuration interaction (SOCI) calculations are employed. Spin–orbit effects were also included for the lowest-lying electronic states using the relativistic CI (RCI) method. All calculations carried out here were made with relativistic effective core potentials (RECPs) which included the outer $5s^25p^1$ shells for In and the outer $5s^25p^3$ shells for Sb in the valence space, respectively.

Valence Gaussian basis sets of $(4s4p1d)$ types shown in Table I for In and Sb were employed in the present study on InSb. The $(3s3p)$ valence Gaussian basis set for In and Sb atoms optimized by LaJohn *et al.*[38] was used as the starting point. To this a set of s, a set of three p functions and one set of six-component d functions with the exponents shown in Table I were added. We used the RECPs generated by LaJohn *et al.*[38] for In and Sb atoms.

CASSCF calculations included all eight outer (valence) electrons of InSb in the active space. All calculations were actually made in the C_{2v} point group orienting the diatomic InSb along the z axis. In this orientation, we included all those orbitals which correlated into the $5s$ and $5p$ orbitals of the separated atoms at infinite separation. Hence the active space for CASSCF included four a_1 orbitals, two b_2 orbitals, and two b_1 orbitals. The calculations of $InSb^+$ and $InSb^-$ included seven and nine active electrons, respectively. At the CASSCF level seven, eight, and nine active electrons were distributed in all possible ways among the eight active orbitals for $InSb^+$, InSb, and $InSb^-$.

CI calculations were made using both first-order CI (FOCI) and full second-order CI (SOCI) methods. The FOCI calculations included (i) all configurations in the CASSCF and (ii) those configurations generated by distributing $N-1$ electrons in the active space and 1 electron in the orthogonal external space in all possible ways, where N is the number of active electrons for various species ($N=7$ for $InSb^+$, $N=8$ for InSb, and $N=9$ for $InSb^-$). The second-order CI (SOCI) calculations included all configurations in the FOCI and those configurations generated by distributing $N-2$ electrons in the active space and two electrons in the external space in all possible ways. The FOCI calculations in the $(4s4p1d)$ basis set included up to 38 000 configurations for those species. The SOCI calculations included up to 700 000 configurations.

Since both In and Sb are heavy atoms spin–orbit effects could be important for InSb. The spin–orbit coupling was introduced variationally allowing for mixing of different electronic states through the relativistic CI (RCI) method described by the author[39] in a previous study.

Spin–orbit integrals in Gaussian basis sets were obtained using Pitzer's modified version of ARGOS codes.[40] The integrals thus obtained were transformed in the CI natural orbitals. The transformed spin–orbit matrix elements were added to the CI Hamiltonian matrix in the RCI procedure.

RCI calculations of the $X0^+$ state of InSb included $^3\Sigma^-_{0^+}(\sigma^2\pi^2)$, $^1\Sigma^+_{0^+}(\sigma^2\pi^2)$, $^3\Pi_{0^+}(\sigma\pi^3)$, $^3\Pi_{0^+}(\sigma^2\sigma^*\pi)$, and $^1\Sigma^+(\pi^4)$ reference configurations. Similarily RCI calculations of the 1 state included $^3\Sigma^-_1$, $^3\Pi_1$, $^1\Pi_1$ and other low-lying states which give rise to $\Omega=1$.

RCI calculations of the $X\,^4\Sigma^-_{1/2}$ state of $InSb^+$ included $^4\Sigma^-_{1/2}$, $^2\Sigma^-_{1/2}$, $^2\Sigma^+_{1/2}$ and a few other states which give $\Omega=1/2$ states. Similarly the $^4\Sigma^-_{3/2}$ state included $^4\Sigma^-_{3/2}$, $^2\Delta_{3/2}$, etc. RCI calculations of $InSb^-$ were also carried out in a similar manner. Spin–orbit splittings of low-lying electronic states were found to be at most 500 cm^{-1} for InSb and $InSb^+$. For $InSb^-$, the contribution is found to be larger due to relativistic $^2\Pi_{1/2}$ and $^2\Sigma^+_{1/2}$ avoided crossing.

All CASSCF/FOCI/SOCI calculations were made using the author's[42] modified version of ALCHEMY II codes[41] to include relativistic ECPs (RECPs)as described in Ref. 42. RCI calculations were carried out using the method described in Ref. 40.

TABLE I. Valence Gaussian basis sets for In and Sb.

Type	In exponent	Sb exponent
s	0.5332	0.5598
s	0.2776	0.4423
s	0.0746	0.1121
s	0.0200	0.0284
p	0.9011	0.9967
p	0.1535	0.2405
p	0.0472	0.0814
p	0.0145	0.0276
d	0.2129	0.1305

III. RESULTS AND DISCUSSION

A. InSb

1. Potential energy curves

Table II shows the possible low-lying electronic states of InSb and their ions together with their dissociation limits. For the neutral InSb potential energy curves of most of the electronic states shown in Table I (with the exception of probably repulsive $^3\Phi$, $^1\Phi$ states and some upper repulsive roots) were calculated. The potential energy curves were calculated using the CASSCF/FOCI methods described in Sec. II.

Figure 1 shows the potential energy curves of InSb arising from $In(^2P)+Sb(^4S)$ and $In(^2P)+Sb(^2D)$ dissociation limits while Fig. 2 shows some states dissociating into $In(^2P)+Sb(^2D)$ and electronic states dissociating into

TABLE II. Dissociation relationship for low-lying electronic states of InSb, $InSb^+$, and $InSb^-$.

Species	States	Dissociation limit
InSb	$^3\Sigma^-$,$^3\Pi$,$^5\Sigma^-$,$^5\Pi$	$In(^2P) + Sb(^4S)$
InSb	$^1\Sigma^+$,$^1\Sigma^-$ (2),$^1\Pi$(3),$^1\Delta$(2),$^1\Phi$, $^3\Sigma^+$,$^3\Sigma^-$ (2),$^3\Pi$(3),$^3\Delta$(2),$^3\Phi$	$In(^2P) + Sb(^2D)$
InSb	$^1\Sigma^+$ (2),$^1\Sigma^-$,$^1\Pi$(2),$^1\Delta$,$^3\Sigma^+$ (2), $^3\Sigma^-$,$^3\Pi$(2),$^3\Delta$	$In(^2P) + Sb(^2P)$
InSb	$^3\Sigma^-$,$^3\Pi$,$^5\Sigma^-$,$^5\Pi$	$In(6p^2P) + Sb(^4S)$
InSb	$^7\Sigma^-$ (2),$^7\Sigma^+$,$^7\Pi$(2),$^7\Delta$, $^5\Sigma^-$ (2),$^5\Sigma^+$,$^5\Pi$(2),$^5\Delta$	$In(^4P) + Sb(^2P)$
$InSb^+$	$^4\Sigma^-$	$In^+(^1S) + Sb(^4S)$
$InSb^+$	$^2\Delta$,$^2\Pi$,$^2\Sigma^-$	$In^+(^1S) + Sb(^2D)$
$InSb^+$	$^2\Pi$,$^2\Sigma^+$	$In^+(^1S) + Sb(^2P)$
$InSb^+$	$^2\Sigma^+$,$^2\Sigma^-$ (2),$^2\Pi$(2),$^2\Delta$,$^4\Delta$, $^4\Sigma^-$ (2),$^4\Pi$(2),$^4\Sigma^+$	$In(^2P) + Sb^+(^3P)$
$InSb^+$	$^4\Pi$,$^4\Sigma^-$	$In^+(^1S) + Sb(^4P)$
$InSb^-$	$^2\Sigma^+$,$^2\Pi$,$^2\Delta$,$^4\Sigma^+$,$^4\Pi$,$^4\Delta$	$In(^2P) + Sb^-(^3P)$
$InSb^-$	$^2\Sigma^+$,$^2\Pi$,$^4\Sigma^+$,$^4\Pi$,$^6\Sigma^+$,$^6\Pi$	$In^-(^3P) + Sb(^4S)$

$In(^2P) + Sb(^2P) + In(6p^2P) + Sb(^4S)$, and $In(^4P) + Sb(^2P)$ dissociation limits.

As seen from Fig. 1, the ground state of InSb is a $^3\Sigma^-$ state. A very low-lying excited $^3\Pi$ state crosses the $^3\Sigma^-$ curve since the R_e of the $^3\Pi$ state is shorter than the R_e of the $^3\Sigma^-$ state. There are $^1\Delta$, $^1\Sigma^+$, and $^1\Pi$ very low-lying excited states for InSb. For the $^1\Sigma^+$ state there is an avoided crossing between the π^4 electronic configuration with the $\sigma^2\pi^2$ configuration. Thus the short-R_e minimum in the $^1\Sigma^+$ curve is due to the π^4 electronic configuration. The different shape of the $^1\Sigma^+$ curve compared to the $^1\Delta$ curve is due to the avoided crossing of π^4 with $\sigma^2\pi^2$. The same way the spectroscopic constants of the $^1\Sigma^+$ and $^1\Sigma^+$(II) states differ from the $^1\Delta$ state. The second $^1\Sigma^+$ state, namely $^1\Sigma^+$(II), has an opposite behavior. It is predominantly $\sigma^2\pi^2$ at short distances and changes to π^4 and other configurations as the internuclear distance increases.

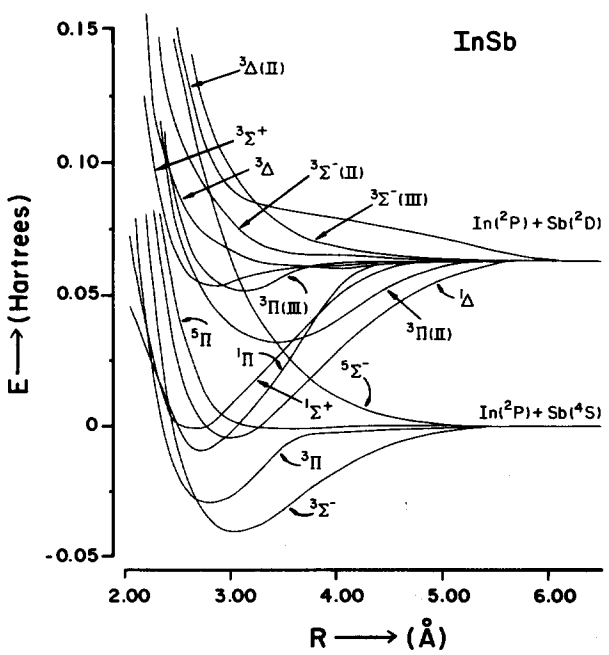

FIG. 1. Potential energy curves of InSb arising from $In(^2P) + Sb(^4S)$ and $In(^2P) + Sb(^2D)$ limits.

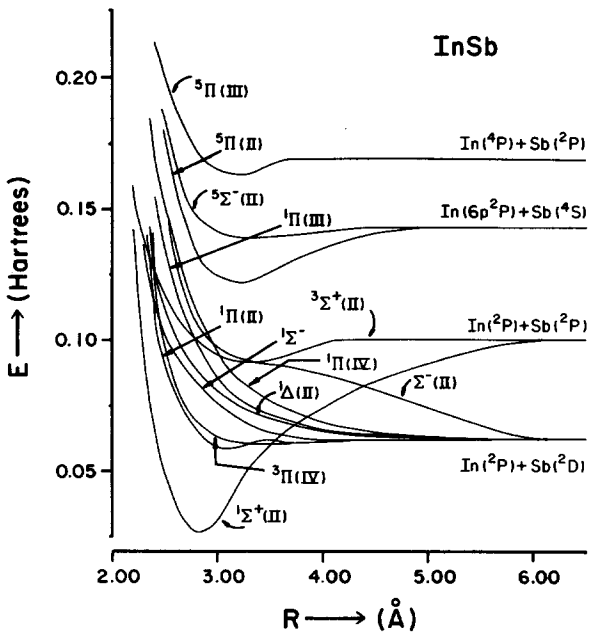

FIG. 2. Potential energy curves of InSb arising from $In(^2P) + Sb(^2D)$, $In(^2P) + Sb(^2P)$, $In(6p^2P) + Sb(^4S)$, and $In(^4P) + Sb(^2P)$ limits.

The quintet states dissociating to the ground state $In(^2P) + Sb(^4S)$ atoms ($^5\Pi$,$^5\Sigma^-$) exhibit interesting behavior. The $^5\Pi$ state is slightly bound while the $^5\Sigma^-$ state is repulsive and crosses the bound $^3\Pi$(II), $^3\Pi$(III), $^3\Sigma^+$, and $^3\Delta$ states (Fig. 1). This would result in the predissociation of the appropriate Ω components. We discuss this in Sec. III A 3.

Among the electronic states dissociating into $In(^2P) + Sb(^2D)$, the $^1\Sigma^+$, $^1\Delta$, $^3\Sigma^+$, $^3\Pi$(II), and $^3\Pi$(III) states are bound while the $^3\Sigma^-$(II), $^3\Sigma^-$(III), and $^3\Delta$(II) states are repulsive. The $^3\Delta$ state is somewhat weakly bound.

The $^3\Pi$(II) curve dissociating into $In(^2P) + Sb(^2D)$ has a broader potential well and a larger R_e. The $^3\Pi$(III) curve dissociating to the same limit, to the contrary, has a shorter R_e and a bit narrower potential well. But the $^3\Pi$(II) state is more bound since the two $^3\Pi$ states dissociate into the same limit (see Fig. 1).

As seen from Fig. 2, the $^1\Sigma^+$(II) curve dissociating into $In(^2P) + Sb(^2P)$ has a deeper and narrower well due to an avoided crossing of $\sigma^2\pi^2$ and π^4 configurations. This curve crosses several curves dissociating into the lower $In(^2P) + Sb(^2D)$ atoms (Fig. 2). In particular the crossing of a repulsive $^3\Pi$ state and subsequently at a longer distance, the crossing of $^3\Sigma^-$(II) are worth noting. Since the $^3\Pi$(IV) curve crosses at a shorter r_e and gives rise to $\Omega = 0^+$ component, the interaction between $^1\Sigma^+(II)_{0^+}$ and $^3\Pi(IV)_{0^+}$ at the curve-crossing region would be strong. This will predissociate the $^1\Sigma^+$(II) state into $In(^2P) + Sb(^2D)$ atoms since InSb is a heavy molecule.

Among those electronic states dissociating into $In(^2P) + Sb(^2P)$, the $^1\Sigma^+$(II) and $^3\Sigma^+$(II) curves are

bound. The $^3\Sigma^+$ (II) curve crosses the $^3\Sigma^-$ (II) repulsive curve near the well and a $^1\Pi$(IV) curve at a shorter r_e. This means that the $^3\Sigma^+$ (II)$_1$ component will be predissociated. The $^3\Sigma^+_{0^-}$ component should survive predissociation since both the curves crossing with $^3\Sigma^+$ (II) do not give rise to $\Omega = 0^-$ states.

We also studied the potential energy curves dissociating into the In($6p^2P$) + Sb(^4S) Rydberg limit. Since our basis set of In is of ($4s4p1d$) quality, the results obtained for Rydberg states may not be of the same accuracy as the ground state but sufficiently satisfactory. This is further evidenced by a CASSCF/FOCI In(^2P)–In($6p^2P$) energy separation of 31 300 cm^{-1} compared to an experimental value of 32 000 cm^{-1}.[43] Thus the accuracy of even electronic states dissociating into Rydberg atoms is quite good. The $^5\Pi$(III) state dissociates into In(^4P) + Sb(^2P).

2. Spectroscopic constants

Table III shows the spin–orbit corrected spectroscopic constants for the bound electronic states of InSb. As seen from Table III, the ground state of InSb is a $X\,^3\Sigma^-_{0^+}$ state with $r_e = 3.02$ Å and $\omega_e = 121$ cm^{-1} at the spin–orbit corrected SOCI level of theory. The FOCI results are also quite satisfactory. The ground state $^3\Sigma^-_{0^+}$–$^3\Sigma^-_1$ spin–orbit splitting is calculated as 492 cm^{-1} using the RCI method. The spin–orbit splitting of the isoelectronic Sn_2 dimer was calculated by the author and Pitzer before as 342 cm^{-1}.[44] (See Ref. 45 for a comparative review of main group dimers and trimers.) The larger spin–orbit splitting of InSb is because Sb makes larger spin–orbit contribution. The r_e and ω_e values for the Sn_2 $X\,^3\Sigma^-_g$ (0^+_g) ground state are 2.76 Å and 197 cm^{-1}, respectively.[44] Thus Sn_2 has a deeper well compared to InSb.

The $X\,^3\Sigma^-_{0^+}$ state of InSb has a slightly longer bond length compared to the $^3\Sigma^-_1$ state. This is primarily because of spin–orbit contamination of $^3\Sigma^-$ ($\sigma^2\pi^2$) with $^1\Sigma^+$ ($\sigma^2\pi^2$) in the $X0^+$ state of InSb. The trend found for InSb is also akin to the corresponding trend for Sn_2.[44] For Sn_2 Δr_e and $\Delta\omega_e$ values for the 0^+ and 1 states are $+0.01$ Å and -8 cm^{-1}. The larger changes in the R_e and ω_e of InSb are consistent with the larger spin–orbit splitting.

TABLE III. Spectroscopic constants of InSb.

State method	R_e (Å) SOCI	R_e (Å) FOCI	T_e (cm^{-1}) SOCI	T_e (cm^{-1}) FOCI	ω_e (cm^{-1}) SOCI	ω_e (cm^{-1}) FOCI	μ_e (D)[a] SOCI
$X\,^3\Sigma^-_{0^+}$	3.02	3.05	0	0	121	115	2.63
$^3\Sigma^-_1$	3.00	3.03	492	492	136	130	2.27
$^3\Pi$	2.769	2.754	2520	2278	158	163	2.295
$^1\Pi$	2.712	2.716	6800	6796	176	177	2.34
$^1\Delta$	2.979	2.977	7150	7702	142	143	1.85
$^1\Sigma^+_{0^+}$	2.56	2.56	8080	7920	189	190	2.6
$^5\Pi$	···	3.74	···	8526	···	34	···
$^1\Sigma^+$(II)	2.807	2.78	13 890	14 776	···	···	···
$^3\Pi$(II)	3.37	3.42	15 930	15 831	68	93	−0.40
$^3\Pi$(III)	···	3.20	···	20 204	···	109	−1.2
$^3\Sigma^+$	2.80	2.80	21 300	20 608	124	130	0.68
$^3\Delta$	···	4.34	···	20 813	···	48	
$^1\Pi$(II)	3.089		21 892		102		
$^3\Pi$(IV)	···	3.36	···	22 315	···	53	
$^3\Delta$(II)	···	3.32	···	28 533	···	76	
$^5\Pi$(II)	···	3.20	···	35 716	···	130	
$^5\Pi$(III)	···	3.13	···	44 565	···	124	

[a] Positive polarity means In^+ Sb^- polarity.

The lowest $^3\Pi$ state of InSb has a shorter r_e of 2.769 Å compared to the ground state. The ω_e is correspondingly larger compared to the ground state. This is consistent with the potential energy curves in Fig. 1. The $^1\Pi$ state of InSb also behaves similar to the $^3\Pi$ state.

The $^1\Delta$ state arising from the $\sigma^2\pi^2$ configuration has spectroscopic properties similar to the $^3\Sigma^-_1$ state since the latter state also arises predominantly from the $\sigma^2\pi^2$ electronic configuration. It is worth noting that if the properties of the $^1\Delta$ state are computed using the $^1A_1$ orbitals, they are somewhat different, since the $^1A_1$ state undergoes an avoided crossing of π^4 and $\sigma^2\pi^2$. As a result the properties of $^1\Delta$ obtained as the second root of $^1A_1$ differ from the properties obtained from the $^1A_2$ first root orbitals. This is an artifact of the change in the $^1A_1$ orbital composition in this region.

The $^5\Pi$ state has a much longer bond length as seen from Table III and Fig. 1. This state is only weakly bound with respect to the ground state atoms.

The $^1\Sigma^+_{0^+}$ state arising predominantly from π^4 at its r_e has a shorter bond length of 2.56 Å as expected for this state. The ω_e is increased for this state due to spin–orbit contamination with $^3\Sigma^-_{0^+}$ by 20 cm^{-1}. The $^1\Sigma^+$ (II) state has a longer bond length of 2.81 Å. The relatively small energy separation between the two $^1\Sigma^+$ states is a result of the avoided crossing of π^4 with $\sigma^2\pi^2$ configurations.

The $^3\Pi$(II) and $^3\Pi$(III) states should be of interest to experimentalists since the corresponding $^3\Pi$(III) state of GaAs has been observed by Lemire *et al.* recently.[15] For InSb at the FOCI level these states lie 15 800 and 20 200 cm^{-1}, respectively, above the ground state. At the more accurate SOCI level of theory, the $^3\Pi$(II) state is 15 930 cm^{-1} above the ground state.

The $^3\Pi$(IV) state lying 22 300 cm^{-1} with a long r_e (3.36 Å) may also be an interesting candidate for experimental studies although this state has a considerably longer bond and is only weakly bound. This state could be observed in absorption.

The $^3\Sigma^+$ state has a shorter r_e (2.80 Å) compared to the $X\,^3\Sigma^-_{0^+}$ ground state but has comparable properties to the $^3\Pi$ state of InSb. Other electronic states of InSb such as $^5\Pi$(II), $^5\Pi$(III), $^3\Delta$(II), etc., have only long range minima and are weakly bound.

Table III compares the SOCI/RCI spectroscopic constants for 11 bound electronic states of InSb with the corresponding FOCI results. SOCI calculations, in general, tend to stabilize the molecular regions of the potential well compared to the dissociation limit thereby enhancing the D_e. For example, the potential well of the $^1\Pi$(II) state is considerably stabilized at the SOCI level.

A critical comparison of the FOCI and SOCI properties reveals that the r_e and ω_e values of the low-lying electronic states of InSb are not altered substantially by the higher-

order electron correlations. The T_e values of the excited electronic states, however, alter due to higher-order correlation effects. The SOCI T_e values should be considered more definitive compared to the FOCI values.

3. Predicted electronic transitions of InSb

There are a number of possible dipole allowed electronic transitions for InSb. From the $X\,^3\Sigma^-_{0^+}$ ground state electronic transitions to the $^1\Pi_1$, $^1\Sigma^+(\mathrm{III})_{0^+}$, $^1\Sigma^+(\mathrm{II})_{0^+}$, $^3\Pi(\mathrm{II})_{0^+}$, $^3\Pi(\mathrm{II})_1$, $^3\Pi(\mathrm{III})_{0^+}$, $^3\Pi(\mathrm{III})_1$, $^3\Pi(\mathrm{IV})_{0^+}$, and $^3\Pi(\mathrm{IV})$, transitions are allowed. Among these, the transitions to the $^3\Pi(\mathrm{II})_{0^+}$ and $^3\Pi(\mathrm{III})_{0^+}$ system would be particularly strong. We discuss these first.

The $^3\Pi(\mathrm{II})_{0^+}$–$X\,^3\Sigma^-_{0^+}$ and $^3\Pi(\mathrm{III})_{0^+}$–$X\,^3\Sigma^-_{0^+}$ transitions occur in the region of 15 800 and 20 200 cm^{-1} at the FOCI level. More accurate T_e of 15 540 cm^{-1} was obtained at the SOCI level for the $^3\Pi(\mathrm{II})$ state. Hence the predicted FOCI $^3\Pi(\mathrm{III})$–$X\,^3\Sigma^-_{0^+}$ transition energy should be about 1200 cm^{-1} in error but in the opposite direction. The spin–orbit splitting is estimated to be less than 1000 cm^{-1} for the two $^3\Pi$ states. Hence the predicted transition energies for the $^3\Pi(\mathrm{II})_{0^+}$–$X\,^3\Sigma^-_{0^+}$ and $^3\Pi(\mathrm{III})_{0^+}$–$X\,^3\Sigma^-_{0^+}$ transitions are 15 500 $\pm$ 500 and 21 700 $\pm$ 1000 cm^{-1}, respectively.

The $^3\Pi(\mathrm{III})$–$X\,^3\Sigma^-_{0^+}$ transition of GaAs was recently observed by Lemire *et al.*[15] The experimental T_e value for this transition was calculated as 23 800 cm^{-1} by these authors. This value was in excellent agreement with a CASSCF/SOCI value of 24 600 cm^{-1} obtained by the author for GaAs before.[21] The theoretical r_e value for the $^3\Pi(\mathrm{III})$ state was calculated as 2.68 Å in good agreement with an experimental value of 2.60 Å. The experimental and theoretical ω_e values of the $^3\Pi(\mathrm{III})$ state are 160 and 152 cm^{-1}, respectively. These results provide considerable confidence in our present CASSCF/SOCI/RCI calculations.

The $^1\Sigma^+(\mathrm{II})_{0^+}$–$X\,^3\Sigma^-_{0^+}$ and $^1\Sigma^+_{0^+}$–$X\,^3\Sigma^-_{0^+}$ transitions become allowed for InSb due to spin–orbit contamination of $^3\Sigma^-$ and $^1\Sigma^+$. The transition energies of the former and latter transitions are 14 000 and 8100 cm^{-1}, respectively.

The $^3\Sigma^+_1$–$X\,^3\Sigma^-_{0^+}$ as well as $^3\Sigma^+_1$–$X\,^3\Sigma^-_1$ transitions are good candidates for theoretical investigations although in a pure λ–s coupling scheme, the $^3\Sigma^+$–$X\,^3\Sigma^-$ transition is forbidden. Since spin–orbit coupling for InSb is strong this transition would be somewhat probable. The $^3\Sigma^+$–$X\,^3\Sigma^-$ transition occurs in the 21 900 cm^{-1} region.

4. Predissociations

As seen from Fig. 1, the repulsive $^5\Sigma^-$ curve dissociating into the $In(^2P) + Sb(^4S)$ atoms crosses the $^1\Delta$, $^1\Sigma^+$, $^1\Pi$, $^3\Pi(\mathrm{II})$, $^3\Pi(\mathrm{III})$, $^3\Sigma^+$, and $^3\Delta$ curves. In the presence of spin–orbit coupling the $^5\Sigma^-$ state gives rise to $\Omega = 0^-$, 1, and 2 states. Since predissociation process is akin to perturbation, two states of the same Ω symmetry can interact through spin–orbit coupling. Depending on the magnitude of the spin–orbit coupling term, the interaction could be strong. Since InSb is a heavy molecule, we expect spin–orbit interaction in the curve crossing region to be large enough to induce predissociation.

The $^5\Sigma^-_{0^-}$ and $^5\Sigma^-_1$ components would predissociate the $^1\Pi_1$, $^3\Pi(\mathrm{II})_1$, $^3\Pi(\mathrm{II})_{0^-}$, $^3\Pi(\mathrm{III})_1$, $^3\Pi(\mathrm{III})_{0^-}$, $^3\Sigma^+_{0^-}$, $^3\Sigma^+_1$, and $^3\Delta_1$ components. Similarly, the $^5\Sigma^-_2$ state would interact with the $^1\Delta_2$, $^3\Pi(\mathrm{II})_2$, $^3\Pi(\mathrm{III})_2$, and $^3\Delta_2$ components. Hence the $^1\Sigma^+$ curve dissociating into $In(^2P) + Sb(^2D)$ would survive predissociation by the $^5\Sigma^-$ curve since the $^5\Sigma^-$ state has no component with 0^+ symmetry.

The $^3\Pi(\mathrm{II})_{0^+}$ and $^3\Pi(\mathrm{II})_{0^+}$ components will survive predissociation induced by the $^5\Sigma^-$ curve crossing since $^5\Sigma^-$ state does not give rise to a state of 0^+ symmetry. Thus among various $^3\Pi(\mathrm{II})$–$X\,^3\Sigma^-_{0^+}$, $^3\Pi(\mathrm{III})$–$X\,^3\Sigma^-_{0^+}$ systems, the $^3\Pi_{0^+}(\mathrm{II})$–$X\,^3\Sigma^-_{0^+}$ and $^3\Pi(\mathrm{III})_{0^+}$–$X\,^3\Sigma^-_{0^+}$ systems would be intense and bands should be observable for several vibrational quantum numbers. For other electronic states in the $^3\Pi$–$X\,^3\Sigma^-$ system only those vibrational levels with classical turning points below the curve crossing r of $^3\Pi(\mathrm{II})$–$^5\Sigma^-$ and $^3\Pi(\mathrm{III})$–$^5\Sigma^-$ could be observed.

The above predictions of predissociations for InSb are consistent with the recently observed predissociation pattern for the GaAs $^3\Pi$–$X\,^3\Sigma^-$ system.[15] Experimentally Lemire *et al.*[15] found no transitions which terminate on $v' > 1$ for $\Omega' = 2$ of the $^3\Pi(\mathrm{III})$ state. Similarly no transitions could be found terminating on $v' > 0$ for $\Omega' = 1$ and $\Omega' = 0^-$ substates of $^3\Pi(\mathrm{III})$. But transitions terminating on $\Omega = 0^+$ substrate were observed. These observations are consistent with earlier comparable calculations on GaAs.[10] In view of the similar predicted predissociation patterns it would be interesting to record the spectrum of InSb in the predicted region.

5. Partition function and dissociation energy of InSb

Theoretical dissociation energy D_e is calculated at various levels of theory through the difference of energy at r_e and long distance (8.0 Å). At the CASSCF/FOCI level, the value obtained this way for D_e (InSb) is 1.1 eV. At a full SOCI level this value improves to 1.35 eV. The zero-point energy obtained from the ω_e of the $X\,^3\Sigma^-_{0^+}$ state is 0.01 eV. Thus the difference between D_e and D_0 for InSb should be approximately 0.01 eV.

Even a full SOCI level of theory ignores the effect of d correlation effects on D_e. In an earlier investigation on GaAs the author estimated the effect of d correlation as an increase in D_e by 0.2 eV. We expect comparable improvement in the D_e of InSb due to d correlation effects. However, spin–orbit effects tend to destabilize the InSb bond by the same factor. Hence D_e (InSb) is predicted as 1.4 $\pm$ 0.1 eV.

De Maria *et al.*[46] have made a thermodynamic study of InSb using a mass spectrometer. The gaseous molecules in equilibrium with solutions of indium and antimony were determined. From the measured partial pressures, partial molar-free energies, the heats of enthalpies in solutions were calculated. These values in turn facilitated the computation of thermodynamic dissociation energies for Sb_2, In_2, InSb, and $InSb_2$. The ω_e of InSb was estimated from the Debye temperature of InSb to be 260 cm^{-1}. The r_e was taken to be 3.15 Å. The ground state of InSb was assumed correctly as $^3\Sigma^-$ in analogy to the well-known ground state of Sn_2. The

$InSb_2$ molecule was assumed to be linear by DeMaria *et al.*[46] The interatomic distance of $InSb_2$ were taken to be r(Sb–Sb) = 2.82 Å and r(In–Sb) = 3.15 Å. Based on these assumptions, average dissociation energies of Sb_2, In_2, InSb, and D_0^0 (InSb–Sb) were calculated as 71.2, 22.4, 35.4, and 66.7 kcal/mol.[46]

Although the assumed ω_e of InSb (260 cm^{-1}) is certainly too high compared to a value of 115–130 cm^{-1} obtained from our calculations, the assumed r_e value (3.15 Å) of InSb is quite reasonable. Thus only the vibrational partition function needs correction.

The D_0^0 obtained by DeMaria *et al.*[46] can be corrected using the formula

$$\delta D_0^0 = RT \ln(q'/q''),$$

where q' is the assumed partition function while q'' is the corrected partition function. Since the main difference between the assumption made by DeMaria *et al.* and our theoretical constants is in the ω_e of InSb, the vibrational partition function was corrected. The δD_0^0 obtained this way for the correction in the vibrational partition function is -1.6 to -1.7 kcal/mol depending on the temperature used (1000–1500 K). Consequently the D_0^0 of InSb should be corrected to 33.4 kcal/mol or 1.45 eV. Note that our direct SOCI D_e of InSb is 1.35. Since the ω_e of InSb in the absence of spin–orbit coupling is 130 cm^{-1}, the D_0 value is obtained by correcting the D_e by zero-point energy as 1.34 eV. As indicated above the d correlation effects tend to increase D_e by 0.2 eV while spin–orbit effects destabilize by about the same factor. The theoretical D_0^0 (InSb) = 1.35 eV obtained this way is in very good agreement with the corrected thermodynamic value of 1.45 eV. Hence D_0^0 (InSb) is predicted as 1.40 ± 0.1 eV.

The assumption of a linear ground state for $InSb_2$ by DeMaria *et al.*[46] is not entirely consistent with the author's earlier[54] calculations on $GaAs_2$ which have revealed $GaAs_2$ to be bent in a $X\,^2B_2$ ground state with a very acute triangular geometry. Furthermore, DeMaria *et al.* have assumed the multiplicity of the ground state to be 1 while it should be 2 for $InSb_2$. In view of these assumptions, the bond energy of D_0(InSb–Sb) could be off to a larger extent compared to D_0^0 (InSb). Theoretical study of $InSb_2$ would thus be quite interesting. Such studies on trimers of In and Sb will be the topic of future investigations.

The present author and Pitzer[44] calculated the D_e value of the isoelectronic Sn_2 using a SCF/RCI method. The D_e value calculated this was 1.86 eV. They also corrected the thermodynamic D_0 value by recalculating the partition functions with theoretical spectroscopic constants for several excited states as $D_0^0 = 44.7$ kcal/mol or 1.94 eV. The corrected $D_0^0(Sn_2)$ was found to be in excellent agreement with the experimental value. The D_0^0(InSb) should be smaller than $D_0^0(Sn_2)$ and since $D_0^0(Sn_2)$ is fairly well established as 1.9 eV, the deduced D_0^0(InSb) = 1.40 ± 0.1 eV is very consistent with the $D_0^0(Sn_2)$.

B. $InSb^+$

1. Potential energy curves and spectroscopic constants

Table IV shows the spectroscopic constants for $InSb^+$ arising from both $In^+ + Sb$ limits and $In + Sb^+$ limits. Figure 3 shows the actual potential energy curves of $InSb^+$. As seen from Table IV and Fig. 3, the ground state of $InSb^+$ is unambiguously a $X\,^4\Sigma^-_{1/2}$ state dissociating into $In^+(^1S) + Sb(^4S_{3/2})$. Since the first ionization potential of the In atom is smaller than the antimony atom, the $In^+(^1S) + Sb(^4S)$ dissociation limit is considerably lower than the $In(^2P) + Sb^+(^3P)$ limit.

The $^4\Sigma^-_{3/2}$–$^4\Sigma^-_{1/2}$ spin–spin splitting is calculated as 327 cm^{-1} comparable to the neutral $^3\Sigma^-_{0^+}$–$^3\Sigma^-_1$ separation of 492 cm^{-1}. The spin–orbit contamination of the $^4\Sigma^-_{1/2}$ state with a low-lying $^2\Sigma^+_{1/2}$ state arising from the same configuration was found to be significant. This result is an increase in the $X\,^4\Sigma^-_{1/2}$ r_e by 0.003 Å. The ω_e correspondingly decreases by 1 cm^{-1}.

The ground state $InSb^+$ is analogous to the $X\,^4\Sigma^-$ ground state for $GaAs^+$ predicted by the author[10] before using comparable level of theory. Knight and Petty[9] subsequently recorded the ESR spectra of matrix-isolated $GaAs^+$ which exhibited a quartet structure confirming the previous theoretical prediction.[10]

An excited electronic state of $^2\Sigma^-$ symmetry arising from the same $\sigma\pi^2$ configuration is found for $InSb^+$. This state lies 8755 cm^{-1} above the ground state. The $^2\Pi$ and $^2\Delta$ electronic states dissociating into $In^+(^1S) + Sb(^2D)$ are immediately above the $^2\Sigma^-$ state.

The next duo of electronic states dissociating into $In^+(^1S) + Sb(^2P)$ of $^2\Sigma^+$ and $^2\Pi$(II) symmetries are found in the 18 000 cm^{-1} region. Since these two states are close to each other, the spin–orbit contamination of the $\Omega = 1/2$ components of $^2\Sigma^+$ and $^2\Pi$(II) states is expected to be significant.

There are many electronic states for $InSb^+$ dissociating into $In(^2P) + Sb^+(^3P)$. The $^4\Pi$ and $^2\Pi$ and $^2\Pi$(III) states dissociating into this limit are bound. The $^2\Delta$(II) state is evidently repulsive (Fig. 3). The $^4\Pi$(II) state exhibits dou-

TABLE IV. Spectroscopic constants of $InSb^+$.

State method	R_e (Å)		T_e (cm^{-1})		ω_e (cm^{-1})		μ_e (D)
	SOCI	FOCI	SOCI	FOCI	SOCI	FOCI	SOCI
$^4\Sigma^-_{1/2}$	3.351	3.203	0	0	63	143	−4.3
$^4\Sigma^-_{3/2}$	3.348	3.200	327	327	64	144	−4.96
$^2\Sigma^-_{1/2}$	2.997	2.934	8 755	9 343	109	84	···
$^2\Pi$	3.407	3.36	9 053	10 098	125	96	···
$^2\Delta$	3.129	3.04	11 155	11 961	75	93	···
$^2\Pi$(II)	2.95	2.90	15 953	17 093	151	177	···
$^2\Sigma^+$	···	2.92	···	18 568	···	104	···
$^4\Pi$	3.039	3.01	26 148	26 470	108	113	···
$^2\Pi$(III)	···	3.34	···	29 704	···	68	···
$^4\Sigma^-$ (II)	2.968	···	29 839	···	148	···	···
$^4\Pi$(II)	···	2.69	···	37 084	···	201	···
$^4\Pi$(III)	···	3.21	···	40 907	···	267	···

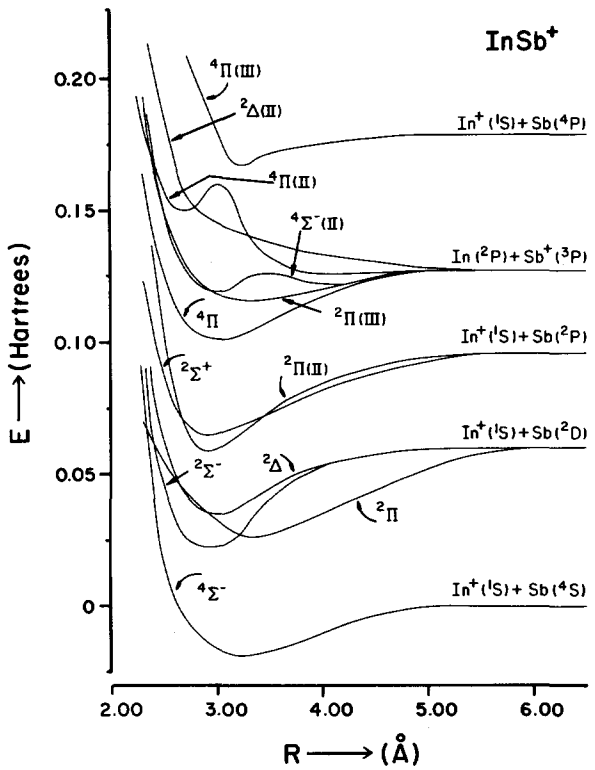

FIG. 3. Potential energy curves of $InSb^+$.

ble minimum in the potential energy curve separated by a barrier (Fig. 3) due to an avoided crossing. All these states lie in the 26 500–37 000 cm^{-1} region as seen from Table IV.

Among various transitions of $InSb^+$, the $^2\Pi$–$X\,^4\Sigma^-_{1/2}$, $^2\Pi(II)$–$X\,^4\Sigma^-_{1/2}$, $^2\Sigma^+$–$X\,^4\Sigma^-_{1/2}$ transitions should be observable in the 10 100–18 600 cm^{-1} region. The $^4\Pi$–$^4\Sigma^-$ transition occurs in the 26 150 cm^{-1} region. Hence if the spectrum of $InSb^+$ could be recorded, it would show these interesting features.

As seen from Table IV, in general, higher-order electron correlation effects not included in the FOCI method tend to destabilize the $InSb^+$ bonding. This is reflected in the longer r_e values obtained at the SOCI level. The ω_e values are correspondingly reduced. The $D_e(InSb^+)$ decreased from a value of 0.52 eV to 0.37 eV at the SOCI level for the $^4\Sigma^-$ state.

The changes in the spectroscopic constants for the $^2\Sigma^-$, $^2\Delta$, $^4\Pi$, and $^4\Sigma^-(II)$ states are somewhat smaller compared to the $^4\Sigma^-$ ground state of $InSb^+$. For example, the r_e value increases by 0.15 Å at the SOCI level compared to the FOCI level of theory. The T_e values are shifted at the most 800 cm^{-1} at the SOCI level of theory.

A D_e value for $InSb^+$ can also be deduced using the following formula:

$$D_e(InSb^+) = \text{I.P.(In)} - \text{I.P.(InSb)} + D_e(InSb).$$

At the FOCI level the values obtained for the above parameters are I.P.(InSb) = 5.92 eV, D_e(InSb) = 1.1 eV, and I.P.(In) = 5.33 eV. Hence $D_e(InSb^+)$ is deduced using the above formula as 0.50 eV. This value is in remarkable agreement with a direct FOCI D_e value of 0.52 eV. Thus internal consistency in the calculations is established. Using the SOCI I.P.(InSb), SOCI D_e(InSb), and SOCI I.P.(In) we obtain $D_e(InSb^+)$ to be 0.3 eV. Again, this value is in excellent agreement with the direct SOCI $D_e(InSb^+)$ of 0.37 eV. Since the SOCI I.P. of the indium atom is closer to an experimental value of 5.79 eV,[43] we believe that SOCI spectroscopic constants should be more accurate.

The accuracy of the present calculations on $InSb^+$ can also be judged by comparable Group IV–VI calculations and experimental photoelectron spectrum of Wang *et al.*[49] In this joint theoretical–experimental study electronic states of PbSe, PbTe, SnSe, SnTe, and their positive ions were studied. The theoretical I.P.s, r_e, ω_e, and D_es were in very good agreement with experimental values. For example, the calculated r_es were found to be within 0.04–0.06 Å of the experimental values. The theoretical ω_es of the Group IV–VI ions were within 2%–6% of experimental values. The MRSDCI I.P.s came very close to experimental values deduced from the photoelectron spectra.

2. Ionization potential and the predicted features in the photoelectron spectrum of InSb

The CASSCF/FOCI adiabatic I.P. of InSb for the following process:

$$InSb(^3\Sigma^-_{0^+}) \rightarrow InSb^+(^4\Sigma^-_{1/2}) + e^-$$

is calculated as 5.92 eV including spin–orbit effects. At a more accurate SOCI/RCI level of theory this value is 6.27 eV.

As seen from Table IV, the Δr_e difference in the ground state of InSb and $InSb^+$ is + 0.15 Å. The increase in the bond length is anticipated since the highest occupied σ orbital of InSb is a bonding MO and hence removal of a bonding electron leads to elongation of the bond. Removal of a π electron then leads to a $^2\Pi$ electronic state for $InSb^+$ which has an $r_e = 3.36$ Å, approximately 0.3 Å larger than the neutral InSb $X\,^3\Sigma^-_{0^+}$ state. This suggests considerable orbital relaxation effects.

The $^2\Sigma^-$ and $^2\Delta$ electronic states of $InSb^+$ have bond lengths close to the $X\,^3\Sigma^-$ ground state of InSb. This means transitions to these states would be sharp. Equivalently, the Franck–Condon factor would be large for this transition.

The electronic transition from the $X\,^3\Sigma^-_{0^+}$ ground state of InSb to the $X\,^4\Sigma^-_{1/2}$ ground state of $InSb^+$ would involve considerable vibrational progression since Δr_e for this transition is + 0.15 Å. Thus the photoelectron spectrum from the ground state of InSb to the ground state of $InSb^+$ should have a smaller Franck–Condon factor and thus the spectrum should show broader peaks exhibiting vibrational progressions.

The $^2\Pi(I)$ state of $InSb^+$ is a mixture of $1\sigma^2 2\sigma^2 3\sigma^2\pi$ (81%) and $1\sigma^2 2\sigma^2\pi^3$ (7%) configurations near the r_e of $InSb^+$. Similarly the $^2\Pi(II)$ state of $InSb^+$ is $1\sigma^2 2\sigma^2\pi^3$ (75%), $1\sigma^2 2\sigma^2 3\sigma^2\pi$ (6%), and other configurations. Note that at the R_e of the neutral InSb ground state (3.05 Å), the $^2\Pi$ state of $InSb^+$ is composed of $1\sigma^2 2\sigma^2 3\sigma^2\pi$ (71%) and $1\sigma^2 2\sigma^2\pi^3$ (16%). At 2.8 Å, the $^2\Pi$ state of $InSb^+$ is made of $1\sigma^2 2\sigma^2 3\sigma^2\pi$ (52%) and $1\sigma^2 2\sigma^2\pi^3$ (33%). Thus the two configurations undergo an avoided crossing which would

result in a complex photoelectron spectra. However, the $^4\Sigma^-$ ground state of InSb is somewhat purer. This situation is analogous to $GaAs^+$. This means the $InSb(X\,^3\Sigma^-) \rightarrow InSb^+$ $[^2\Pi, ^2\Pi(II)]$ transitions would be comprised of satellite peaks analogous to the predicted photoelectron spectrum for GaAs.[10,16,21] The separation between $^2\Pi$ and $^2\Pi(II)$ states of $InSb^+$ is only 6800 cm^{-1} at the SOCI level of theory. This is the primary reason for the strong interaction of $1\sigma^2 2\sigma^2 3\sigma^2\pi$ and $1\sigma^2 2\sigma^2\pi^3$ configurations of $InSb^+$.

C. $InSb^-$

1. Potential energy curves and spectroscopic constants

Figure 4 shows the potential energy curves of $InSb^-$ obtained using a full CASSCF/FOCI method. Although the FOCI calculations included up to 38 000 configurations we do not expect the FOCI calculations to be as accurate as the SOCI calculations especially for $InSb^-$.

As seen from Fig. 4, there are virtually degenerate electronic states for $InSb^-$ of $^2\Sigma^+$ and $^2\Pi$ symmetries. The $^2\Pi$ state has a slightly longer bond length compared to the $^2\Sigma^+$ state ($\Delta R_e = 0.05$ Å). The $^2\Pi$–$^2\Sigma^+$ energy separation of $InSb^-$ at the FOCI level is only 58 cm^{-1}. Hence the ground state of $InSb^-$ cannot be established unambiguously at this level of theory.

The existence of two nearly degenerate states for $InSb^-$ makes it more interesting since the $^2\Sigma^+_{1/2}$ state undergoes an avoided crossing with the $^2\Pi_{1/2}$ state as a result of near-degeneracy of these states and larger spin–orbit coupling for $InSb^-$ compared to the lighter analogs in this group of compounds.

As seen from Table V, when spin–orbit effects are included through the RCI method, the $X\,^2\Pi_{3/2}$ state is the ground state of $InSb^-$. The $^2\Pi$ state arises from the $1\sigma^2 2\sigma^2 3\sigma^2\pi^3$ configuration and is thus an inverted $^2\Pi$. Consequently, the $^2\Pi_{3/2}$ component is lowered with respect to $^2\Pi$ by 1075 cm^{-1}.

The $^2\Sigma^+_{1/2}$ state undergoes considerable spin–orbit mixing with the nearly degenerate $^2\Pi_{1/2}$ state. This increases the R_e of the $^2\Sigma^+_{1/2}$ state by 0.06 Å. The ω_e sharply drops due to the strong contamination with $^2\Pi$. The $^2\Sigma^+_{1/2}$ state is effectively lowered due to this spin–orbit contamination. Effectively, it lies 484 cm^{-1} above the $^2\Pi_{3/2}$ state. The designation $^2\Sigma^+_{1/2}$ is thus crude and the correct designation for this state is 1/2(I).

The 1/2(II) state approximately exhibits an opposite behavior compared to the 1/2 state. Its R_e decreases by the same factor (0.06 Å) while the ω_e increases by the same factor due to spin–orbit mixing. This state is raised with respect to the $^2\Pi$ state as expected for an inverted $^2\Pi$ state. Thus $InSb^-$ is quite interesting from the standpoint of relativistic effects.

The $^4\Pi$ excited state of $InSb^-$ has a long bond length ($\sim$3.4 Å) and a correspondingly smaller ω_e. This is anticipated for a high spin state of a negative ion such as $InSb^-$.

The $^4\Delta$ and $^4\Sigma^-$ states have relatively shorter bond lengths compared to the $^4\Pi$ state. These states are approximately 12 000–13 500 cm^{-1} above the ground state of $InSb^-$.

The crossing of many electronic states for $R = 2.8$–3.0 Å would make the spectrum very complex in this region (see Fig. 4). The $^4\Pi(II)$ state is predominantly repulsive.

The $^2\Pi(II)$, $^2\Sigma^+(II)$, and $^2\Delta$ excited states of $InSb^-$ are relatively more bound compared to the quartet states. The existence of 9 or more low-lying bound electronic states for $InSb^-$ below 15 000 cm^{-1} is consistent with the corresponding states of $GaAs^-$.[21]

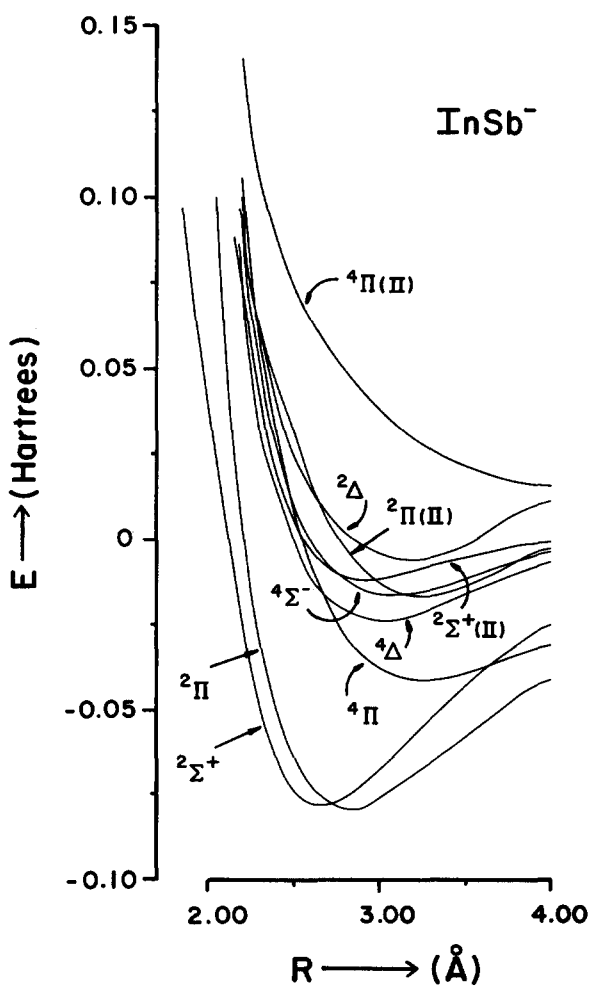

FIG. 4. Potential energy curves of $InSb^-$.

TABLE V. Spectroscopic constants of $InSb^-$.

State method	R_e (Å)		T_e (cm^{-1})		ω_e (cm^{-1})	
	SOCI	FOCI	SOCI	FOCI	SOCI	FOCI
$X\,^2\Pi_{3/2}$	2.776	2.705	0	0	230	187
$^2\Sigma^+_{1/2}$	2.646	2.72	884	484	189	142
$^2\Pi_{1/2}$	2.721	2.65	2 615	2 615	293	240
$^4\Pi$	···	3.4	···	7 882	···	74
$^4\Delta$	···	3.01	···	11 794	···	121
$^4\Sigma^-$	···	3.13	···	13 422	···	96
$^2\Pi(II)$	···	3.22	···	13 445	···	108
$^2\Sigma^+(II)$	···	2.90	···	14 405	···	185
$^2\Delta$	···	3.18	···	15 589	···	130

The predicted spectroscopic constants and potential energy curves of $InSb^-$ would be especially of interest to experimentalists pursuing negative photoelectron or photodetachment spectra of anions. For example, Lineberger and co-workers[50–52] have carried out similar studies on many species to obtain electron affinities and to probe the electronic states of the neutral species. Since $InSb^-$ is well bound, the negative photoelectron spectrum of $InSb^-$ could be a possible method to study the predicted electronic states of neutral InSb.

2. Electron affinity and dissociation energy for $InSb^-$

The FOCI/RCI adiabatic electron affinity of InSb for the process

$$InSb(^3\Sigma^-_{0^+}) + e^- \rightarrow InSb^-(^2\Pi_{3/2})$$

is calculated as 1.0 eV. It is well known that electron correlation effects tend to have significant impact on electron affinities. A full SOCI/RCI adiabatic E.A. of InSb is 1.39 eV.

The electron affinity of the In atom as deduced from the long distance calculations at the SOCI/RCI level is 0.3 eV in excellent agreement with an experimental value of 0.32 eV obtained by Hotop and Lineberger.[50] As listed by Hotop and Lineberger,[50] the antimony atom has a larger electron affinity of 1 eV. This is manifested in the molecular region of the electronic states of $InSb^-$ as we discuss in a subsequent section on Mulliken populations. That is the negative charge of $InSb^-$ resides more on the antimony atom than on the In atom as the E.A. of Sb is greater than the In atom.

The dissociation energy of $InSb^-$ was computed as the difference of its energy at r_e and at a long distance of 8.0 Å. At the FOCI level of theory the value obtained this way is 2.1 eV. At the same level of theory the neutral InSb has a D_e of 1.1 eV (see Sec. III A 5). Thus at the FOCI level of theory $InSb^-$ is 1 eV more bound compared to the neutral InSb.

At the full SOCI level, the $D_e(InSb^-)$ is calculated as 2.5 eV. Since SOCI calculations are more accurate then FOCI calculations, we predict that $D^0_0(InSb^-) = 2.7 \pm 0.2$ eV.

It can be seen from the predicted D_0 and E.A. of $InSb^-$ and InSb, respectively, that there is a difference of ~ 1.3 eV between $D_0(InSb^-)$ and E.A.(InSb). This means that those electronic states of the neutral InSb lying < 1.3 eV of the ground state of InSb could be probed using negative ion photoelectron spectroscopy of $InSb^-$. Thus $^3\Pi$, $^1\Pi$, $^1\Delta$, $^5\Pi$, and $^1\Sigma^+$ states of InSb should be accessible for experimental photodetachment studies.

IV. ANALYSES OF WAVE FUNCTIONS AND THE NATURE ON LOW-LYING ELECTRONIC STATES OF InSb, $InSb^+$, AND $InSb^-$

A. Dipole moments

Tables III and IV show the dipole moments of the low-lying electronic states of InSb and $InSb^+$, respectively, obtained at the SOCI level near the equilibrium geometries of the respective states. Note that dipole moments of charged species are gauge dependent. In all cases the dipole operator was placed on the In atom.

All low-lying electronic states of InSb ($^3\Sigma^-$, $^3\Pi$, $^1\Pi$, $^1\Sigma^+$, $^1\Delta$) are very ionic with In^+Sb^- polarity. The $X\,^3\Sigma^-$ ground state has a large dipole moment of 2.3 D in the absence of spin–orbit coupling. This value is much larger compared to the isoelectronic GaAs for which the $X\,^3\Sigma^-$ ground state has a dipole moment of 1.34 D.

Since the spin–orbit coupling term mixes the $^3\Sigma^-_{0^+}$ ($\sigma^2\pi^2$) with $^1\Sigma^+_{0^+}$ ($\sigma^2\pi^2$), the μ_e value of the $X0^+$ state of InSb is expected to be altered as the r_e value changes significantly due to the spin–orbit contamination. Hence relativistic density matrices and properties were obtained using the enhancement to our RCI codes described in Ref. 53. Table III also shows the dipole moments of the $X\,^3\Sigma^-_{0^+}$ and $^3\Sigma^-_1$ states including the effects of spin–orbit coupling. The spin–orbit contamination of the $^3\Sigma^-_{0^+}$ state with the $^1\Sigma^+_{0^+}$ state increases the dipole moment by almost 0.33 D since the bond length of $X\,^3\Sigma^-_{0^+}$ increases due to this contamination. Hence, spin–orbit mixing has a large contribution to the dipole moment of InSb. It would be quite interesting to measure the μ_e of InSb in the $X0^+$ ground state.

The $^3\Sigma^-_1$ state to the contrary is not influenced much by spin–orbit coupling since contamination with the low-lying $^3\Pi_1$ and $^1\Pi_1$ states add up to only 0.2%. Thus $\Delta\mu_e^{SO}$ for the $X\,^3\Sigma^-_1$ state is -0.034 D.

The dipole moment of the $^3\Pi$ state is a bit larger than the $X\,^3\Sigma^-$ state in the absence of spin–orbit coupling. Note that the μ_e value of GaAs in the $^3\Pi$ state at the SOCI level is 1.61 D.[21]

The dipole moments of the excited electronic states of InSb such as $^3\Pi$(II) and $^3\Pi$(III) have opposite polarity (In^-Sb^+). This suggests that the $^3\Pi$(II)–$X\,^3\Sigma^-$ and $^3\Pi$(III)–$X\,^3\Sigma^-$ transitions of InSb involve considerable charge transfer. This trend for InSb is akin to the corresponding trend for GaAs.[21]

The dipole moments of $InSb^+$ are large and negative. Since the dipole operator was placed on the In atom the negative value suggests that significant portion of the positive charge resides on the In atom. As we discuss later this is consistent with the Mulliken population charge distributions.

The dipole moments of the $^2\Sigma^+$ and $^2\Pi$ electronic states of $InSb^-$ are large and positive. The positive polarity suggests that significant portion of the negative charge is on the Sb atom in $InSb^-$. This is fully consistent with the experimental electron affinities of In (0.3 eV) and Sb (1 eV) listed by Ho and Lineberger.[50] Thus Sb would preferably keep the electron compared to the indium atom.

B. Composition of the CI wave functions of InSb, $InSb^-$, and $InSb^+$

1. InSb

The compositions of the CI wave functions of electronic states of InSb are of interest. The ground state of InSb ($^3\Sigma^-$) is found to be predominantly composed of the $1\sigma^2 2\sigma^2 3\sigma^2 1\pi^2$ configuration (87%) and configuration spin functions arising from the $1\sigma^2 2\sigma^2 1\pi^2 2\pi^2$ (3%). The 1σ and 2σ orbitals are predominantly Sb($5s$) and In($5s$), respectively. The 2σ or-

bital is a mixture of Sb($5p_z$) and In($5p_z$). The 1π orbital is found to be a predominantly Sb($5p$) orbital. There is significantly smaller contribution by the In($5p$) orbital to the 1π orbital. The 2π orbital to the contrary is composed predominantly of the In($5p$) orbital. The occupancies of the $1\pi_x$ and $1\pi_y$ orbitals add up to 1.979 while the occupancy of the 3σ orbital is 1.894. This makeup of orbitals is consistent with In^+Sb^- ionic character of the bonds.

The $^3\Pi$ and $^1\Pi$ states are predominantly composed of the $1\sigma^2 2\sigma^2 3\sigma 1\pi^3$ (81%, 73%) configuration. The $^1\Delta$ state is composed mainly of the $1\sigma^2 2\sigma^2 3\sigma^2 1\pi^2$ configuration (88%).

The first two $^1\Sigma^+$ states exhibit interesting trends as a function of internuclear distance. At small distances, the $^1\Sigma^+$(I) state is predominantly $1\sigma^2 2\sigma^2 1\pi^4$ (75%) although mixing with $1\sigma^2 2\sigma^2 3\sigma^2 1\pi^2$ is significant near the short r_e of this state (7%). At very short distance ($R = 2.2$ Å), the $^1\Sigma^+$ state is 83% $1\sigma^2 2\sigma^2 1\pi^4$, 2.5% $1\sigma^2 3\sigma^2 \pi^4$, and only 2.5% $1\sigma^2 2\sigma^2 3\sigma^2 1\pi^2$. At 2.90 Å $^1\Sigma^+$(I) becomes $1\sigma^2 2\sigma^2 3\sigma^2 \pi^2$ (40%), $1\sigma^2 2\sigma^2 3\sigma\pi^4$ (19%), and $1\sigma^2 2\sigma^2 \pi^4$ (14%). Thus the $^1\Sigma^+$ state undergoes an avoided crossing of $1\sigma^2 2\sigma^2 \pi^4$ with $1\sigma^2 2\sigma^2 3\sigma^2 \pi^2$ which is reminiscent of the corresponding state of GaAs.[10,21]

The $^1\Sigma^+$(II) state exhibits approximately an opposite orthogonal behavior to the $^1\Sigma^+$(I) state. At 2.2 Å it is 74% $1\sigma^2 2\sigma^2 3\sigma^2 1\pi^2$ and 3% $1\sigma^2 2\sigma^2 \pi^4$. At 2.70 Å, it is 67% $1\sigma^2 2\sigma^2 3\sigma^2 \pi^2$ and 10% $1\sigma^2 2\sigma^2 \pi^4$. At 2.90 Å the $^1\Sigma^+$(II) state becomes 35% $1\sigma^2 2\sigma^2 3\sigma^2 1\pi^2$, 20% $1\sigma^2 2\sigma 3\sigma 1\pi^4$, and 17% $1\sigma^2 2\sigma^2 1\pi^4$. Hence among various states of InSb, the $^1\Sigma^+$ states exhibit the most interesting behavior as a function of internuclear distance.

The high-lying states of InSb such as $^3\Sigma^+$(II), $^1\Sigma^-$, etc., also are complex mixtures of $1\sigma^2 2\sigma^2 1\pi^3 2\pi$ and $1\sigma^2 2\sigma^2 3\sigma^2 1\pi 2\pi$ configurations. The $^3\Pi$(II), and $^3\Pi$(III) states which are potential candidates for experimental studies are also mixtures of $1\sigma^2 2\sigma^2 3\sigma 1\pi^2 2\pi$, $1\sigma^2 2\sigma^2 3\sigma 1\pi^3$, and other configurations.

2. $InSb^+$

The ground state of $InSb^+$ is predominantly made of the $1\sigma^2 2\sigma^2 3\sigma 1\pi^2$ configuration. The $^2\Sigma^-$ and $^2\Delta$ states of $InSb^+$ arise from the same configuration.

Among various electronic states of $InSb^+$ the $^2\Pi$ state and the $^4\Sigma^-$(II) state exhibit interesting compositions leading to avoided crossings and somewhat different shapes of potential energy curves for these states. At short distances ($R < 3$ Å) the $^2\Pi$ state of $InSb^+$ is a mixture of $1\sigma^2 2\sigma^2 1\pi^3$ (53%) and $1\sigma^2 2\sigma^2 3\sigma^2 1\pi$ (33%) although the former configuration dominates. At longer distances ($R \sim 3.5$ Å) this state becomes predominantly $1\sigma^2 2\sigma^2 3\sigma^2 \pi$. The $^2\Pi$(II) state exhibits an opposite behavior. Near 2.7 Å these two configurations make almost equal contributions to the two $^2\Pi$ states. As discussed in Sec. III B 2, this would result in complex photoelectron spectral bands corresponding to transitions terminating into these states.

The $^4\Sigma^-$(II) state is a mixture of $1\sigma^2 2\sigma^2 3\sigma^2 1\pi^2$, $1\sigma^2 2\sigma^2 3\sigma 1\pi 2\pi$, and $1\sigma^2 2\sigma 3\sigma^2 1\pi 2\pi$ configurations at shorter distances. The contributions from Rydberg configurations are also quite noticeable at these distances. At longer distances this state becomes significantly $1\sigma^2 2\sigma^2 4\sigma 1\pi^2$. Consequently, there is an avoided crossing in this state which leads to minima (second one relatively weak) separated by a barrier (see Fig. 3). Thus the photoelectron spectrum corresponding to InSb ($X\,^3\Sigma^-$) $\rightarrow$ $InSb^+$ [$^4\Sigma^-$(II)] would be quite interesting in that it would exhibit features corresponding to quantum tunneling and predissociation. The crossing of the $^2\Delta$(II) repulsive curve would predissociate the $^4\Sigma^-(II)_{3/2}$ component but the $^4\Sigma^-(II)_{1/2}$ state should survive.

3. $InSb^-$

The two low-lying electronic states of negative ion of InSb are relatively simple in characters from the standpoint of CI composition in the absence of spin–orbit coupling. The $^2\Pi$ and $^2\Sigma^+$ states of $InSb^-$ are predominantly composed of the $1\sigma^2 2\sigma^2 3\sigma^2 \pi^3$ and $1\sigma^2 2\sigma^2 3\sigma 1\pi^4$ configurations. The mixing of $1\sigma^2 2\sigma^2 3\sigma 1\pi^2 2\pi^2$ configurations (3.4%) is quite noticeable in the $^2\Sigma^+$ state.

C. Mulliken populations

Table VI shows Mulliken population analyses of the low-lying electronic states of InSb, $InSb^+$, and $InSb^-$. In that table, we have omitted the d and s populations. The s populations are between 1.4 and 1.7 for In and close to 2.0 for Sb in most of the states. The d populations add up to 0.20.

The $X\,^3\Sigma^-$ ground state of InSb is composed of In ($s^{1.69}p^{0.75}$) and Sb ($s^{2.03}p^{3.32}$). Note that the s population of Sb is almost 2.0 suggesting the inertness of the Sb $5s^2$ shell in the bond formation. For the In atom however, there is more $5s$ orbital participation. This is also seen from the actual composition of the 3σ orbital of InSb. The larger Sb p population and an overall Sb population of 5.38 suggests an excess of 0.38 electrons on the antimony atom in the $X\,^3\Sigma^-$ state of InSb. This is fully consistent with the calculated dipole moment of InSb which suggests In^+Sb^- polarity of bonds.

The $^3\Pi$(II) and $^3\Pi$(III) states of InSb have substantially larger In populations compared to both the $X\,^3\Sigma^-$ ground state and $^3\Pi$ state. These are consistent with the predicted

TABLE VI. Mulliken population analyses of InSb, $InSb^+$, and $InSb^-$.

		Gross population				
Species	State	In	Sb	In(p)	Sb(p)	Overlap
InSb	$^3\Sigma^-$(I)	2.62	5.38	0.75	3.32	0.16
InSb	$^3\Pi$(I)	2.66	5.34	0.93	3.27	0.46
InSb	$^1\Pi$(I)	2.68	5.32	1.07	3.24	0.60
InSb	$^1\Delta$(I)	2.64	5.36	0.77	3.30	0.19
InSb	$^1\Sigma^+$(I)	2.71	5.29	1.10	3.27	0.66
InSb	$^1\Sigma^+$(II)	2.73	5.27	0.94	3.25	0.31
InSb	$^3\Pi$(II)	2.92	5.08	1.31	3.01	−0.10
InSb	$^3\Pi$(III)	3.02	4.98	1.30	2.93	0.05
$InSb^+$	$^4\Sigma^-$	2.31	4.69	0.35	2.80	0.1
$InSb^+$	$^2\Pi$	2.25	4.75	0.35	2.80	0.178
$InSb^+$	$^2\Pi$(II)	2.18	4.82	0.35	2.80	0.178
$InSb^-$	$^2\Sigma^+$	3.19	5.81	1.52	3.73	0.734
$InSb^-$	$^2\Pi$	3.14	3.86	1.27	3.78	0.429

charge transfers in the $X\,^3\Sigma^- \rightarrow {}^3\Pi(III)$ and $X\,^3\Sigma^- \rightarrow {}^3\Pi(II)$ transitions. Similarly the $^1\Pi(II)$ state has larger In population. The In ($5p$) population is noticeably larger for the $^3\Pi(II)$, $^3\Pi(III)$, and $^3\Sigma^+$ states.

The total In and Sb Mulliken populations in the $^4\Sigma^-$, $^2\Pi$, and $^2\Pi(II)$ states of $InSb^+$ are approximately 2.2–2.3 and 4.7–4.8, respectively. This suggests that 70%–75% of the positive charge resides on the indium atom in InSb. The experimental I.P.s of In and Sb are 5.79 and 8.64 eV, respectively.[43] Thus the Mulliken populations and dipole moments of $InSb^+$ are fully consistent with the fact that the I.P. of Sb is substantially larger than that of In.

The total In and Sn population of the $^2\Sigma^+$ and $^2\Pi$ states of $InSb^-$ are 3.14–3.19 and 5.81–5.86, respectively. This suggests that nearly 81%–85% of the negative charge is on the antimony atom in $InSb^-$ electronic states. Note that experimental electron affinities of In and Sb are 0.3 and 1 eV, respectively.[50] Hence since antimony has greater electron affinity, most of the negative charge shifts to the Sb atom in $InSb^-$.

The In–Sb overlap populations approximately depend on the r_e values although for repulsive states the overlaps are negative. Thus the In–Sb overlap is larger for the neutral $^3\Pi$ state compared to the $X\,^3\Sigma^-$ state (Table VI). The overlap populations of the negative ionic states are larger than the neutral states, while the overlaps of the positive ionic states are reduced. This is consistent with the strengthening of the In–Sb bond in the former case while in the latter case In–Sb bond is weakened.

D. RCI wave functions and spin–orbit contamination

The compositions of the RCI wave function of the low-lying electronic states of $InSb^-$ are quite interesting. Spin–orbit mixings of electronic states of InSb and $InSb^+$ are small.

The 1/2(I) state of $InSb^-$ exhibits a very interesting trend as a function of internuclear distance. At 2.5 Å, the 1/2 state is composed of 86% $^2\Sigma^+_{1/2}$ ($1\sigma^2 2\sigma^2 3\sigma 1\pi^4$) and 12% $^2\Pi_{1/2}$ ($1\sigma^2 2\sigma^2 3\sigma^2 1\pi^3$). At 2.7 Å it becomes 56%–35% mixture of these two states. At 2.8 Å the composition reverses to 35% $^2\Sigma^+_{1/2}$ and 56% $^2\Pi_{1/2}$. Consequently, not only the spin–orbit contamination of $^2\Sigma^+_{1/2}$ and $^2\Pi_{1/2}$ is large in these states but they undergo avoided crossings. The 1/2(II) of $InSb^-$ state exhibits an opposite behavior.

The $X\,^3\Sigma^-_{0^+}$ ground state of InSb is 92% $^3\Sigma^-$, 3% $^1\Sigma^+$, and only 0.1% $^3\Pi_{0^+}$. Both $^3\Sigma^-$ and $^1\Sigma^+$ arise from the same $1\sigma^2 2\sigma^2 3\sigma^2 1\pi^2$ configurations. Thus spin–orbit contamination is significant even in the ground state of InSb.

The $InSb^+$ is composed of 91% $^4\Sigma^-_{1/2}$ and 1.4% $^2\Sigma^+_{1/2}$ at 3.5 Å. Thus spin–orbit contamination is less in $InSb^+$ compared to the neutral InSb $X\,^3\Sigma^-_{0^+}$ state. Hence spin–orbit contamination is the largest for InSb and the smallest for $InSb^+$. The near-degeneracy of the $^2\Sigma^+$ and $^2\Pi$ states is the primary factor which is responsible for the significant spin–orbit mixing of $^2\Sigma^+_{1/2}$ with $^2\Pi_{1/2}$ in the case of $InSb^-$.

V. COMPARISON OF InSb AND GaAs

Table VII shows a comparison of selected spectroscopic constants of electronic states of GaAs with InSb and the corresponding ions. As evidenced from Table VII, the calculated R_es of InSb are approximately 0.4 Å longer than the corresponding values for GaAs. The ω_e values are correspondingly smaller. This is anticipated for the heavier InSb.

The energy separations of valence electronic state of InSb in the absence of spin–orbit coupling are in general quite comparable although for the lowest-lying electronic states, T_es of InSb states are larger than the corresponding values for GaAs.

The T_e values of the $^3\Pi(II)$ and $^3\Pi(III)$ states of InSb are roughly 2300–3000 cm^{-1} smaller than the corresponding values for GaAs. This is mainly due to the fact that the J-weighted ^4S–^2D separation for Sb is 9317 cm^{-1} while the corresponding separation for As is 10 786 cm^{-1}.[43] Since both the $^3\Pi(II)$ and $^3\Pi(III)$ electronic states of InSb arise from $In(^2P) + Sb(^2D)$, the smaller T_e values of the $^3\Pi(II)$ and $^3\Pi(III)$ states of InSb compared to GaAs is understable.

The I.P., E.A., and D_e of GaAs at the best level of theory are 6.9, 1.3, and 1.9 eV, respectively. The corresponding SOCI/RCI values for InSb are 6.33, 1.41, and 1.45 eV, respectively. The smaller D_e for InSb is quite understable for a heavier diatomic.

Since most of the positive charge of the $InSb^+$ ion resides on the indium atom, the I.P. relationship of GaAs to InSb should correspond to the corresponding I.P. relationship of Ga and In atoms. The I.P.s of Ga and In are 6.0 and 5.79 eV, respectively.[43] Hence the I.P. of InSb should be smaller than the I.P. of GaAs. This is in accord with our theoretical I.P.s of these species.

As discussed before, most of the negative charge of $InSb^-$ is localized on the antimony atom. The E.A. of As and Sb are 0.81 and 1.08 eV, respectively.[50] Thus the E.A. (InSb) should be larger than E.A. (GaAs). Note that this quantitative argument is consistent with the SOCI E.A.s of these two species.

TABLE VII. Comparison of selected properties of GaAs, $GaAs^+$, and $GaAs^-$ with InSb, $InSb^+$, and $InSb^-$.[a]

	R_e (Å)		ω_e (cm^{-1})		T_e (cm^{-1})	
State	GaAs	InSb	GaAs	InSb	GaAs	InSb
			MG (V)			
$^3\Sigma^-$	2.55	3.0	214	120	0	0
$^3\Pi$	2.38	2.77	236	157	1 830	2 500
$^1\Pi$	2.34	2.72	277	176	6 440	6 800
$^1\Sigma^+$	2.23	2.56	279	189	7 768	8 080
$^3\Pi(II)$	3.10	3.37	135	68	18 590	15 930
$^3\Sigma^+$	2.405	2.80	208	124	23 403	21 308
$^3\Pi(III)$	2.68	3.20	160	109	23 800	20 200
			MG (V)$^+$			
$^4\Sigma^-$	2.94	3.35	89	64	55 250	51 056
$^2\Sigma^-$	2.519	3.00	250	109	64 957	59 811
$^2\Pi$	3.06	3.36	120	96	65 750	60 110
			MG (V)$^-$			
$^2\Sigma^+$	2.268	2.646	303	189	− 8 100	− 10 489
$^2\Pi$	2.426	2.776	216	230	− 7 300	− 11 373

[a] MG (V) stands for either GaAs or InSb.

Based on the above comparison of the properties of InSb and GaAs, we predict the properties of heavier species in this group, namely, TlBi. Since the I.P. of Tl is 6.1 eV,[43] the I.P. of TlBi is expected to be larger than InSb. The change in the I.P. trend of Tl is primarily due to the larger spin–orbit effects which stabilize the $^2P_{1/2}$ ground state of Tl compared to the $^1S_0$ closed shell ground state of Tl^+. The D_e (TlBi) is expected to be substantially reduced compared to the D_e (InSb) mainly due to spin–orbit destabilization. We predict that D_e(TlBi) < 0.7 eV. The bond lengths of the electronic states of TlBi would also be considerably longer.

The electron affinity of the Bi atom is 0.95 eV and hence is only a bit smaller than the Sb atom.[50] Hence the E.A. (InSb) and E.A. (TlBi) should be comparable.

Since the $^4S_{3/2}$–^2D separation for Bi is 11 400–15 400 cm^{-1}, we predict that the $^3\Pi$(II)–$X\,^3\Sigma_{0^+}^-$ transition energies of TlBi should be larger than the corresponding energies for InSb.

VI. CONCLUSION

In this investigation potential energy curves and spectroscopic constants of 26 electronic states of InSb, 12 electronic states of $InSb^+$, and 9 electronic states of $InSb^-$ were obtained using a complete active space SCF (CASSCF) followed by FOCI and SOCI calculations which included up to 700 000 configurations. The ground state properties of InSb, $InSb^+$, and $InSb^-$ were calculated as

InSb $X\,^3\Sigma_{0^+}^-$: $R_e = 3.02$ Å, $\omega_e = 121\ cm^{-1}$, $D_e = 1.35$ eV,
$X\,^3\Sigma_1^-$: $R_e = 3.03$ Å, $\omega_e = 136\ cm^{-1}$, $T_e = 494\ cm^{-1}$;
$InSb^+$ $X\,^4\Sigma_{1/2}^-$: $R_e = 3.35$ Å, $\omega_e = 63\ cm^{-1}$, $D_e = 0.37$ eV;
$InSb^-$ $X\,^2\Pi_{3/2}$: $R_e = 2.695$ Å, $\omega_e = 191\ cm^{-1}$, $D_e = 2.5$ eV.

Many spectroscopic transitions in the IR–UV regions are predicted for InSb. Specifically the $^3\Pi$(II)–$X\,^3\Sigma^-$ and $^3\Pi$(III)–$X\,^3\Sigma^-$ transitions are predicted at 15 900 and 20 200 cm^{-1} regions, respectively. Both the $^3\Pi$(II) and $^3\Pi$(III) states were found to be predissociated. Thermodynamic D_0^0(InSb) is corrected by reevaluating the partition function of InSb as 1.45 eV. The dipole moments of $X\,^3\Sigma_{0^+}^-$, $X\,^3\Sigma_1^-$, and $^3\Pi$ states of InSb are calculated at the SOCI level of theory as 2.63, 2.27, and 2.3 D, respectively, with In^+Sb^- polarity.

The adiabatic I.P. and E.A. of InSb are calculated as 6.33 and 1.41 eV, respectively. The $^2\Sigma_{1/2}^+$ and $^2\Pi_{1/2}$ states of $InSb^-$ undergo avoided crossing due to the near-degeneracy of these states. Most of the positive charge resides on In in the $X\,^4\Sigma_{1/2}^-$ ground state of $InSb^+$ while most of the negative charge resides on Sb in the $^2\Pi$ ground state of $InSb^-$. More bound electronic states below 15 000 cm^{-1} are found for $InSb^-$ compared to the neutral InSb molecule.

ACKNOWLEDGMENT

This research was supported in part by the U.S. National Science Foundation under Grant No. CHE8818869.

[1] S. C. O'Brien, Y. Liu, Q. L. Zhang, F. K. Tittel, R. F. Curl, and R. E. Smalley, J. Chem. Phys. **84**, 4074 (1986).
[2] Y. Liu, Q. L. Zhang, F. K. Tittel, R. F. Curl, and R. E. Smalley, J. Chem. Phys. **85**, 7434 (1986).
[3] M. L. Mandich, W. D. Reents, Jr., and V. E. Bondybey, in *Atomic and Molecular Clusters*, edited by E. Bernstein (Elsevier, Amsterdam, 1990).
[4] K. Balasubramanian, Chem. Rev. (in press).
[5] R. E. Smalley, in *Cluster Spectroscopy*, edited by E. R. Bernstein (Elsevier, Amsterdam, in press).
[6] J. C. Phillips, Chem. Rev. **86**, 619 (1986).
[7] V. E. Bondybey, W. D. Reents, and M. L. Mandich (unpublished results).
[8] M. Rasanen, C. A. Heimbrook, G. P. Schwartz, and V. E. Bondybey, J. Chem. Phys. **85**, 86 (1986).
[9] L. Knight and J. T. Petty, J. Chem. Phys. **88**, 481 (1988).
[10] K. Balasubramanian, J. Chem. Phys. **86**, 3410 (1987).
[11] K. Balasubramanian, Chem. Phys. Lett. **150**, 71 (1988).
[12] K. Balasubramanian, J. Chem. Phys. **87**, 3518 (1987).
[13] K. Balasubramanian, J. Mol. Spectrosc. **121**, 465 (1987).
[14] W. J. Reents, Jr., J. Chem. Phys. **90**, 4258 (1989).
[15] G. W. Lemire, G. A. Bishea, S. A. Heidecke, and M. D. Morse, J. Chem. Phys. (in press).
[16] U. Meier, S. D. Peyerimhoff, P. J. Bruna, and F. Grien, J. Mol. Spectrosc. **134**, 259 (1989).
[17] K. Balasubramanian, J. Phys. Chem. **85**, 3401 (1986).
[18] K. Balasubramanian, J. Mol. Spectrosc. **123**, 228 (1987).
[19] K. Balasubramanian and J. Q. Li, J. Chem. Phys. **88**, 4979 (1988).
[20] U. Meier, S. D. Peyerimhoff, P. S. Bruna, S. R. Karna, and F. Grien, Chem. Phys. (in press).
[21] K. Balasubramanian, J. Mol. Spectrosc. **139**, 405 (1990).
[22] K. D. Kolenbrander and M. Mandich, J. Chem. Phys. (in press).
[23] P. F. Bernath, S. A. Rogers, L. C. O'Brien, C. R. Brazier, and A. D. McLean, Phys. Rev. Lett. **60**, 197 (1988).
[24] C. A. Stwarts, W. A. Goddard III, and T. C. McGhill, J. Vac. Sci. Technol. **19**, 551 (1981).
[25] K. Balasubramanian, Chem. Phys. Lett. **150**, 71 (1988).
[26] R. G. Wheeler, K. LaiHing, W. L. Wilson, and M. A. Duncan, Chem. Phys. Lett. **113**, 8 (1986).
[27] Q. Zhang, Y. Liu, R. F. Curl, F. K. Tittel, and R. E. Smalley, J. Chem. Phys. **88**, 1670 (1988).
[28] M. A. Duncan (private communication).
[29] L. Knight, Jr. (private communication).
[30] K. Raghavachari, J. Chem. Phys. **84**, 5672 (1986).
[31] K. Raghavachari and V. Logovinsky, Phys. Rev. Lett. **55**, 2583 (1985).
[32] K. Raghavachari and C. M. Rohlfing, J. Chem. Phys. **89**, 2219 (1988).
[33] K. Balasubramanian, Chem. Phys. Lett. **125**, 400 (1986).
[34] R. S. Grev and H. F. Schaefer III, Chem. Phys. Lett. **119**, 111 (1985).
[35] K. Balasubramanian, Chem. Phys. Lett. **135**, 287 (1987).
[36] K. Raghavachari and C. M. Rohlfing, Chem. Phys. Lett. **143**, 428 (1988).
[37] G. Pacchioni and J. Koutecky, J. Chem. Phys. **84**, 3301 (1986).
[38] L. A. LaJohn, P. A. Christiansen, R. B. Ross, T. Atashroo, and W. C. Ermler, J. Chem. Phys. **87**, 2812 (1987).
[39] K. Balasubramanian, J. Chem. Phys. **89**, 5131 (1988).
[40] R. M. Pitzer and N. W. Winter, J. Phys. Chem. **92**, 3061 (1988).
[41] The major authors of ALCHEMY II are B. Liu, B. Lengsfield, and M. Yoshimine.
[42] K. Balasubramanian, Chem. Phys. Lett. **127**, 585 (1986).
[43] C. E. Moore, *Tables of Atomic Energy Levels*, (National Bureau of Standards, Washington, D.C., 1971), Vol. III.
[44] K. Balasubramanian and K. S. Pitzer, J. Chem. Phys. **78**, 321 (1983).

[45] K. Balasubramanian, Chem. Rev. **90**, 93 (1990).
[46] G. Demaria, J. Drowart, and M. G. Ingram, J. Chem. Phys. **31**, 1076 (1959).
[47] K. Balasubramanian and J. Q. Li, J. Mol. Spectrosc. **135**, 169 (1989).
[48] K. P. Huber and G. Herzberg, *Constants of Diatomic Molecules* (van Nostrand, New York, 1979).
[49] L. S. Wang, B. Niu, Y. T. Lee, D. A. Shirley, and K. Balasubramanian, J. Chem. Phys. **92**, 899 (1990).
[50] H. Hotop and W. C. Lineberger, J. Phys. Chem. Ref. Data **14**, 731 (1985).
[51] D. G. Leopold, J. Ho, and W. C. Lineberger, J. Chem. Phys. **86**, 1715 (1987).
[52] K. M. Ervin, J. Ho, and W. C. Lineberger, J. Chem. Phys. **89**, 4514 (1988).
[53] K. Balasubramanian, J. Chem. Phys. **91**, 2443 (1989).
[54] K. Balasubramanian, J. Chem. Phys. **87**, 3518 (1987).